

## A study on bending strength of reinforced concrete filled steel tubular beam

Alifujiang Xiamuxi <sup>\*1</sup>, Akira Hasegawa <sup>2a</sup> and Akenjiang Tuohuti <sup>1b</sup>

<sup>1</sup> College of Architecture and Civil Engineering, Xinjiang University, Urumqi 830047, China

<sup>2</sup> Department of Environmental and Civil Engineering, Hachinohe Institute of Technology, Hachinohe, Japan

(Received November 08, 2013, Revised February 08, 2014, Accepted February 15, 2014)

**Abstract.** The mechanical characteristic of reinforced concrete filled steel tubular (RCFT) structures are differed from that of concrete filled tubular steel (CFT) structures because the reinforcement in RCFT largely affects the performance of core concrete such as ductility, strength and toughness, and hence the performance of RCFT should be evaluated differently from CFT. To examine the effect axial reinforcement on bending performance, an investigation on RCFT beams with varying levels of axial reinforcement is performed by the means of numerical parametric study. According to the numerical simulation results with 13 different ratios of axial reinforcement, it is concluded that the reinforcement has obvious effect on bending capacity, and the neutral axis of RCFT is different from CFT, and an evaluation equation in which the effect of axial reinforcement is considered for ultimate bending strength of RCFT is proposed.

**Keywords:** RCFT; axial reinforcement; numerical simulation; neutral axis; bending strength

---

### 1. Introduction

Concrete filled tubular steel (CFT) structures have gained popularity in supporting heavy loads in high rise buildings, bridges and offshore structures due to their excellent seismic event resistant structural properties such as high strength, high ductility and large energy absorption capacity. Along with the realization of merits of CFT in engineering works, CFT members with bending and tension also started to become very popular.

As a variation of CFT structures, reinforced concrete filled steel tubular (RCFT) structures appeared soon after the Hanshin-Awaji earthquake of Japan in 1995, as a reinforcement method for heavily damaged reinforced concrete (RC) and steel tube piers. Since then, RCFT structures are grown up in the process of practical application and research works. Fig. 1 illustrates the models of CFT and RCFT.

RCFT structures are developed mainly on the purpose of combining the merits of RC and CFT structures. Known research results and application examples until now (Endo *et al.* 2000, Sato 2008, Tanigaki *et al.* 2002, Suzuki 2008, Wang *et al.* 2002, Wei *et al.* 2005, Xiamuxi and

---

\*Corresponding author, Doctor of Engineering, E-mail: [ilikyurt@xju.edu.cn](mailto:ilikyurt@xju.edu.cn)

<sup>a</sup> Professor, E-mail: [hasegawa@hi-tech.ac.jp](mailto:hasegawa@hi-tech.ac.jp)

<sup>b</sup> Professor, E-mail: [akjt@xju.edu.cn](mailto:akjt@xju.edu.cn)

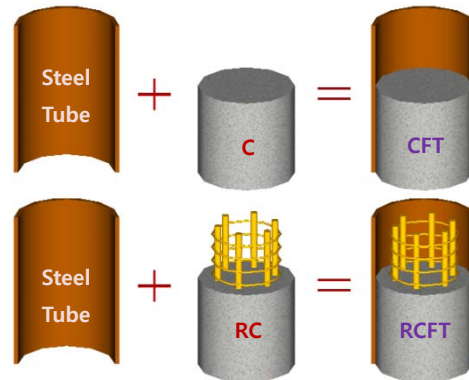


Fig. 1 Models of CFT and RCFT

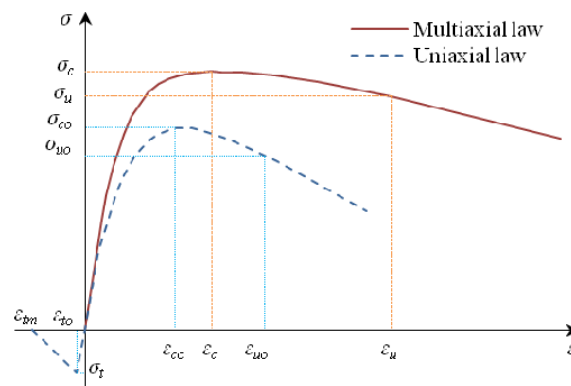


Fig. 2 Constitutive law for concrete

Hasegawa 2011) proved that bearing capacity, toughness, ductility and seismic performance of RCFT structures are increased compared with those of CFT. In other words, because of the existence of reinforcement, the performance of RCFT differed from that of CFT, and hence the evaluation methods for the performance of CFT cannot be completely applied to RCFT.

In order to examine the effect of axial reinforcement on bending performance, in this study, an investigation on RCFT beams with varying levels of axial reinforcement is performed by the means of numerical parametric study. According to the numerical simulation results with 13 different ratios of axial reinforcement, the behaviors of RCFT under pure bending were studied and discussed.

## 2. Numerical model and validation

### 2.1 Numerical model

#### 2.2.1 Material model for concrete

A multiaxial stress-strain law, used in this study, for concrete core is shown in Fig. 2.

It is well known that when the concrete is subjected to laterally confining pressure, the compressive strength and the corresponding strains are much higher than those of unconfined concrete. In RCFT, the lateral pressure is provided by both steel tube and reinforcements, thus, we assumed that the strength  $\sigma_c$  and corresponding strain  $\varepsilon_c$  of concrete core in RCFT may be the multiple of the strength  $\sigma_{co}$  and corresponding strain  $\varepsilon_{co}$  of unconfined concrete, respectively, which can be expressed as

$$\sigma_c = k_c \cdot \sigma_{co} \tag{1a}$$

$$\varepsilon_c = k_{\varepsilon c} \cdot \varepsilon_{co} \tag{1b}$$

where  $k_c$  and  $k_{\varepsilon c}$  is increase parameter for strength and corresponding strain of concrete core due to the confinement effect of both steel tube and reinforcement, respectively. According to Xiamuxi and Hasegawa (2012),  $k_c$  and  $k_{\varepsilon c}$  can be defined using following empirical equations

$$k_c = 5.71\gamma_s^2 - 2.96\gamma_s + 1.62 \tag{1c}$$

$$k_{\varepsilon c} = 0.94 \exp(3.9\gamma_s) \tag{1d}$$

in which  $\gamma_s$  is the load-sharing ratio of RCFT and should be defined using the equation proposed by Xiamuxi and Hasegawa (2012) or see Eq. (13).

Based on the  $\sigma_c$  and  $\varepsilon_c$ , we defined the ultimate strength  $\sigma_u$  and corresponding strain  $\varepsilon_u$  of concrete core, respectively, as

$$\sigma_u = k_u \cdot \sigma_c \tag{2a}$$

$$\varepsilon_u = k_{\varepsilon u} \cdot \varepsilon_c \tag{2b}$$

where the  $k_u$  is a degradation parameter for strength of concrete core, and  $k_{\varepsilon u}$  is a parameter to define ultimate strain. According to Xiamuxi and Hasegawa (2012),  $k_c$  and  $k_{\varepsilon c}$  can be defined using following empirical equations

$$\begin{aligned} k_u &= 3.4\gamma_s - 0.05 & \gamma_s \leq 0.3 \\ k_u &= 1.0 & \gamma_s > 0.3 \end{aligned} \tag{2c}$$

$$k_{\varepsilon u} = 5.6 \tag{2d}$$

Thus, the constants  $\sigma_c$ ,  $\sigma_u$ ,  $\varepsilon_c$ ,  $\varepsilon_u$  can be employed in order to completely define, using the equations for stress-strain relationship proposed in ADINA (2008), the multiaxial stress-strain law (see Fig. 2).

Post-crack tension hardening is considered by an unloading branch after  $\varepsilon_{10}$ , and assume that the tensile stress of the concrete is linearly released to zero at  $\varepsilon_{1m}$ , where  $\varepsilon_{1m} = \zeta \varepsilon_{10}$ , and there is no standard value for  $\zeta$ . In this study, referring to Soranakom and Mobasher (2007) and Chen *et al.* (2008) a value  $\zeta = 8.0$  is used.

To simulate multiaxial compressive and tensile failure of the concrete core in RCFT, considering the simplicity of the model, in this study, a linearized Kupfer model (Kupfer *et al.* 1969) illustrated as Fig. 3 is used after the validation against complex triaxial failure envelopes (ADINA 2008).

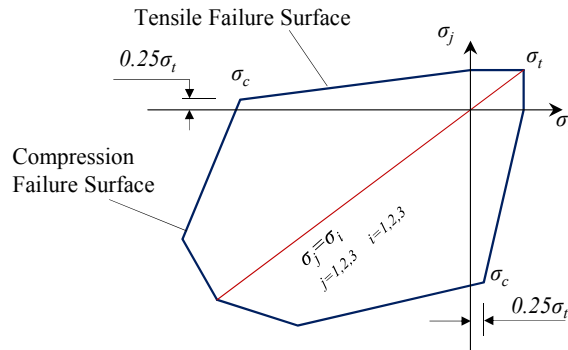


Fig. 3 Failure envelopes

In Fig. 3, the failure surfaces are defined using following equations

$$\sigma_{ce} = \frac{1 + 3.65\alpha}{(1 + \alpha)^2} \sigma_c \quad 0 \leq \alpha = \frac{\sigma_i}{\sigma_j} \leq 1 \quad (3a)$$

$$\sigma_{te} = \left( 1 - 0.75 \frac{\sigma_{j \text{ or } i}}{\sigma_c} \right) \sigma_t \quad (3b)$$

where  $\sigma_{ce}$  and  $\sigma_{te}$  are the effective stresses on compression and tensile failure surfaces, respectively;  $\sigma_i$  and  $\sigma_j$  are principal stresses in corresponding directions 1,2 and 3;  $\alpha$  is principal stress ratio, and set to 0.75 in this study.

Throughout the section, some constant parameters for uniaxial stress-strain relationship can be determined as follows:

$\sigma_{co}$  can be taken by material test and corresponding value of  $\varepsilon_{co}$  is usually around the range of 0.002 to 0.003, a representative value suggested by ACI Committee 318 (1999) used in the analysis is  $\varepsilon_{co} = 0.003$ .

$\sigma_{to}$  or  $\sigma_t$  is determined by  $\sigma_t = 0.23(\sigma_c)^{2/3}$  according to JSCE (2007).

$E_o$  is highly correlated to its compressive strength and can be calculated with reasonable accuracy from the empirical equation by ACI Committee 318 (1999)

$$E_o = 4700\sqrt{\sigma_c} \quad (4)$$

The Poisson's ratio  $\nu_c$  of concrete under uniaxial compressive stress ranges from 0.15 to 0.22, with a representative value of 0.19 or 0.20 by ASCE (1982). In this study,  $\nu_c$  is set to be  $\nu_c = 0.20$ .

### 2.1.2 Material model for steel

The response of the steel tube is modeled by an elastic-perfectly-plastic theory with associated flow and isotropic hardening rule. When the stress points fall inside the yield surface, the behavior of the steel tube is linearly elastic. If the stresses of the steel tube reach the yield surface, the behavior of the steel tube becomes perfectly plastic. Consequently, the steel tube is assumed to fail

and cannot resist any further loading if the stresses of the steel tube are beyond the elastic limit, and a von Mises yield criterion is employed to define the elastic limit, which is written as

$$\sigma_e = \sqrt{3J_2} = \sqrt{\frac{(\sigma_1 - \sigma_2)^2 + (\sigma_2 - \sigma_3)^2 + (\sigma_1 - \sigma_3)^2}{2}} \tag{5}$$

where  $J_2$  is second stress invariant of the stress deviator tensor and  $\sigma_1$ ,  $\sigma_2$ , and  $\sigma_3$  are principal stresses.

A constitutive law with von Mises yield criterion for this model is shown as Fig. 4, values for yield stress  $f_{sy}$ , yield strain  $\epsilon_{sy}$ , and maximum allowable plastic strain  $\epsilon_{su}$  are obtained from uniaxial material tests. Poisson’s ratio  $\nu_s$  and Young’s modulus  $E_s$  are set to  $\nu_s = 0.3$  and  $E_s = 200$  GPa, respectively.

**2.1.3 Reinforcement modeling**

Axial and lateral reinforcements are modeled with truss elements. The lines are defined as truss elements and connected to solid elements (concrete) through the constraint equations (ADINA 2008), as shown in Fig. 5. The constraint equations take form as

$$U_k = \sum_j \alpha_j U_j \tag{6}$$

where  $U_k$  is a dependent (slave) degree of freedom which is controlled by multiple independent (master)  $U_j$  degrees of freedom via factors  $\alpha_j$ . And the reinforcement is set as master, the concrete is set as slave.

**2.1.4 Contact modeling**

The treatments in simulating the contact between steel tube and concrete in numerical analysis of CFT vary between the researchers. There have been examples of bond, frictional and frictionless contact models. Choi and Yan (2010) adopted frictionless contact condition in CFT columns under axial compression with ADINA. Hu *et al.* (2003) modeled the contact in CFT with infinitesimal sliding and friction between the concrete and the steel tube. The contact surfaces between the concrete and the steel tube are allowed to separate but not to penetrate each other. The friction

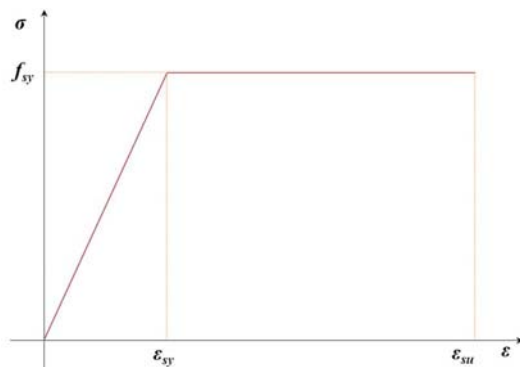


Fig. 4 Constitutive law for steel

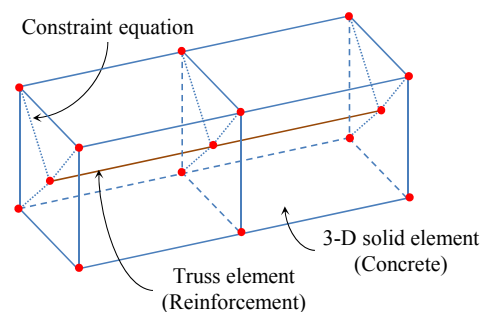


Fig. 5 Reinforcement modeling

coefficient used in their analyses was 0.25. Han *et al.* (2007) employed Coulomb friction theory with a friction coefficient of 0.6 in contact modeling of CFT subject to torsion. Zeng *et al.* (2011) employed Coulomb friction theory with a friction coefficient of 0.6 in simulating the contact between stitches and concrete. Hou *et al.* (2011) employed Coulomb friction theory with a friction coefficient of 0.6 in contact modeling of CFT subject to impact force. Mao and Wang (2011) assumed complete bond between steel tube and concrete in modeling the steel-concrete composite beam joints. Kwak *et al.* (2011) simulated cyclic behavior of CFT columns with bonded contact condition. All of those indicate that the treatments of contact between steel tube and concrete differed greatly between the researchers, and it is difficult to find any standard for the friction between the concrete and steel materials.

In this study, then, we performed the simulations of RCFT beams with frictionless, frictional and bonding contact conditions between, and observed that only the bonding condition showed better agreement against the experiment. Hence, a constraint-function model built in ADINA (2008) with bonding contact condition is employed to simulate contact between steel tube and concrete.

### 2.1.5 Modeling of RCFT beams

The steel tube is defined using geometric pipe body, concrete core is defined using geometric cylinder body, and both axial and lateral reinforcements are defined using geometric lines. The geometric bodies are meshed with 10-node 3-D solid elements employing Delaunay meshing algorithm provide in ADINA (2008). Through a plenty of trial and error procedures, we found that better speed and accuracy can be achieved with element size 15 mm, and correspondingly element edge length for bodies and lines is set to 15 mm for mesh densities.

## 2.2 Validation

Bending test results of RCFT and CFT beams by Sato (2008) are used to validate the numerical model for bending. The formation of the beams is illustrated in Fig. 6. Materials are used as follows: Steel tube is SS400 (JIS) with yield strength  $f_{sy} = 314$  MPa and thickness is  $t = 3.2$  mm; Axial reinforcement is SD295 with yield strength  $f_{sr} = 352$  MPa and diameter  $d_s = 6.0$  mm; Lateral

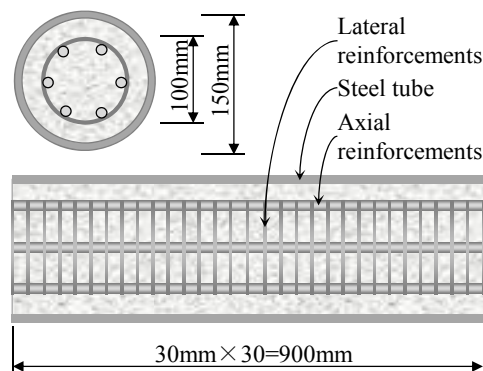


Fig. 6 Formation of RCFT beams

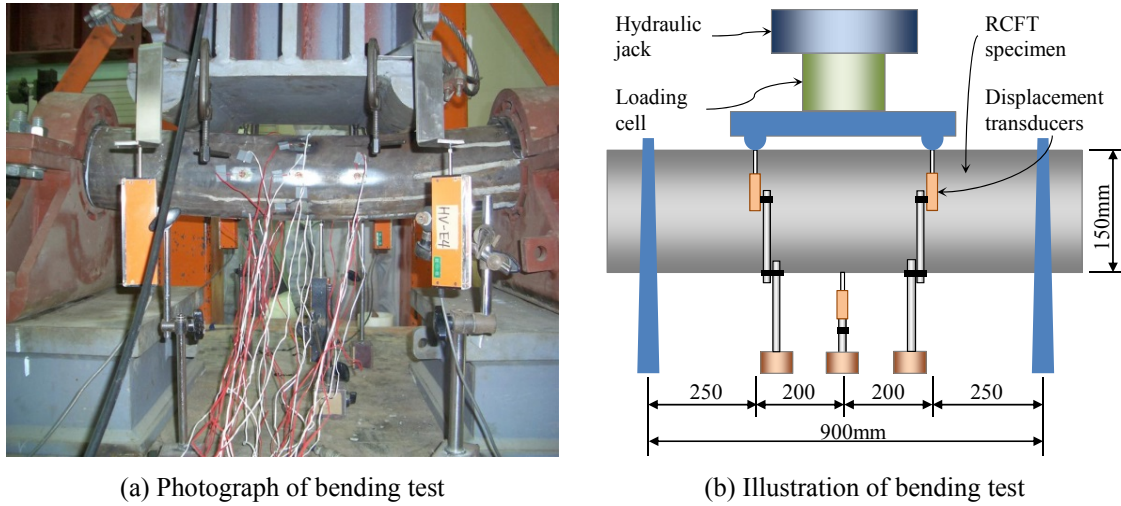


Fig. 7 Bending test

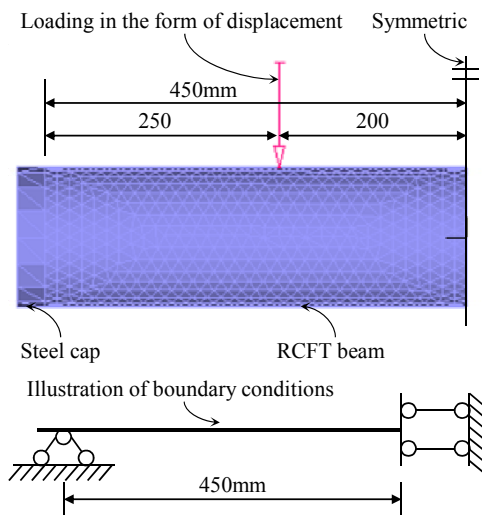


Fig. 8 Illustrations of bending simulation

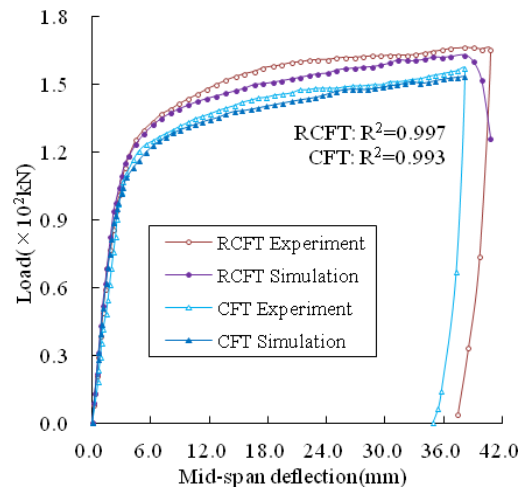


Fig. 9 Validation of bending model against experiment

reinforcement is SS400 with yield strength  $f_{sl} = 304$  MPa and diameter  $d_s = 3.0$  mm; Uniaxial strength of concrete is  $\sigma_{co} = 27.1$  MPa. Fig. 7 shows the photograph of support condition and illustration of test, and Fig. 8 illustrates the numerical model.

The results of the simulations are plotted in Fig. 9. The correlation coefficient  $R^2$  between the load-deflection curves of experiment and numerical simulation of RCFT and CFT beams are  $R^2 = 0.997$  and  $R^2 = 0.993$ , respectively, which means the numerical results match with experimental results very well.

### 3. Effect of axial reinforcement

#### 3.1 Parameters

To examine the effect of axial reinforcement on bending performance of RCFT, using the numerical simulation model in previous section, numerical analyses are carried out on RCFT beams with varying ratios of axial reinforcement.

The size of RCFT beams, material, arrangement and number of both axial and lateral reinforcements are kept same as in previous section. The varying ratio of axial reinforcement  $\rho$  for RCFT beams is determined based on the specifications of JSCE (2007) on the range of  $\rho$  for RC columns, namely  $0.8\% \leq \rho \leq 6.0\%$ , and other two smaller values than 0.8% are also used considering extra small  $\rho$  for RCFT. Only one type of steel tube is used, and its thickness  $t$  is set to  $t = 1.2$  mm. The concrete is used as  $\sigma_{co} = 40.80$  MPa. The determined 13 values for  $\rho$  and the corresponding labels for numerical analyses are listed in Table 1.

#### 3.2 Results and discussions

##### 3.2.1 Discussions on ratio of axial reinforcement

The values of bending strength  $\sigma_M$  (stress values on the compression flange of steel tube which were obtained from the one element of steel tube at mid-span section where the maximum stresses will happen in theory) are listed in Table 1 and plotted against  $\rho$  in Fig. 10. The bending strength is increasing along with the increase of  $\rho$ , but the increase is stopped at  $\rho = 3.0\%$  with  $\sigma_M = 310$  MPa, which is maybe assumed that when the reinforcement is in a proper level, a better balance of strength between steel tube and reinforcement supposed to be achieved, thus, the flange of steel tube yields at the same time as reinforcement yields. But, this balance may be broken with an extra amount of reinforcement (say  $\rho > 3.0\%$ ) that the compression flange of steel tube started to local buckling and yield while the reinforcement just started to raise its best performance. Again, although  $\sigma_M$  increases with the increase of  $\rho$  until  $\rho = 3.0\%$ , but the increment is very small (say 1.1 MPa in average), which means that RCFT members with circular sections are more pressure proof other than bending.

The bending ductility  $\mu_\psi$  can be the ratio of plastic curvature  $\psi_u$  against yield curvature  $\psi_y$ , namely,  $\mu_\psi = \psi_u / \psi_y$ .  $\psi_y$  and  $\psi_u$ , herein, is determined based on the mid-span deflections corresponding to the yield and plastic strain of compression flange of steel tube, respectively, and the plastic strain then is selected as 4 times of yield strain based on the material test of steel tube (Xiamuxi and Hasegawa 2011). The calculated values of  $\mu_\psi$  are listed in Table 1 and plotted against  $\rho$  in Fig. 11. Again, the bending toughness  $\chi_{c,b}$  is calculated based on the curves of stress versus strain at compression edge of concrete core (the values of stress-strain herein were obtained from the one element of concrete at mid-span section where the maximum stresses will happen in theory), and the values of  $\chi_{c,b}$  are listed in Table 1 and plotted against  $\rho$  in Fig. 12. Both  $\mu_\psi$  and  $\chi_{c,b}$  are starting increase after  $\rho = 1.5\%$  and decrease after  $\rho = 3.0\%$ , namely, RCFT with bending is showing better performance between  $1.5\% \leq \rho \leq 3.0\%$ .

Summarizing discussions above, it can be concluded that the ratio of axial reinforcement has the effect on bending performance of RCFT members, and there would be an optimal range for the ratio of axial reinforcement which would help the steel tube and concrete to improve their performance and also put RCFT into better mechanical and economic condition, and this optimal range, in this study, can be proposed as  $1.5\% \leq \rho \leq 3.0\%$ .

Table 1 Simulation results with bending

Labels	$P$ (%)	$\sigma_M$ (MPa)	$\varphi_y$ (m <sup>-1</sup> )	$\varphi_u$ (m <sup>-1</sup> )	$\mu_\psi$	$\chi_{c,b}$ ( $\times 10^6$ J/m <sup>3</sup> )
CFT	0.0	296.6	0.033	0.123	3.69	0.53
PB-R02	0.2	298.1	0.042	0.162	3.82	0.61
PB-R04	0.4	299.9	0.033	0.129	3.85	0.65
PB-R08	0.8	302.9	0.042	0.164	3.86	0.66
PB-R11	1.1	304.6	0.042	0.165	3.89	0.65
PB-R15	1.5	306.1	0.033	0.130	3.91	0.69
PB-R20	2.0	307.5	0.042	0.165	3.92	0.72
PB-R25	2.5	308.5	0.042	0.166	3.94	0.73
PB-R30	3.0	309.5	0.042	0.165	3.95	0.72
PB-R35	3.5	310.0	0.042	0.164	3.94	0.68
PB-R40	4.0	310.1	0.042	0.164	3.93	0.67
PB-R44	4.4	310.1	0.042	0.163	3.94	0.68
PB-R50	5.0	310.2	0.041	0.163	3.94	0.67
PB-R60	6.0	310.3	0.041	0.162	3.94	0.65

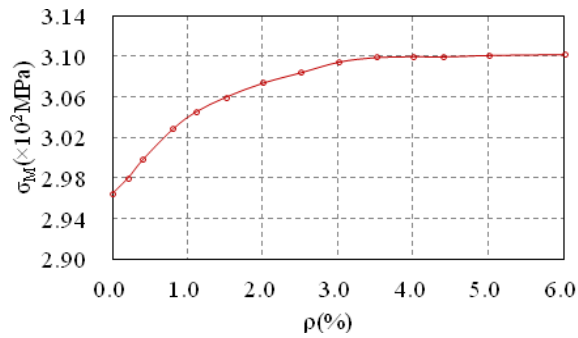


Fig. 10 Bending strength versus reinforcement ratio

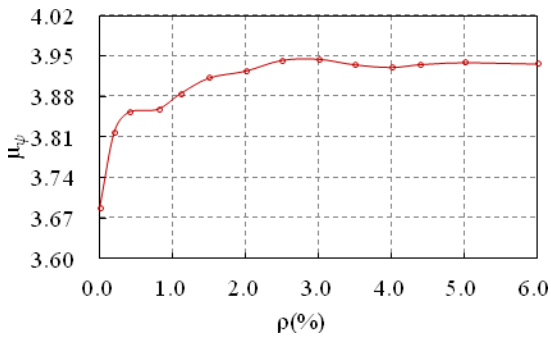


Fig. 11 Bending ductility versus reinforcement ratio

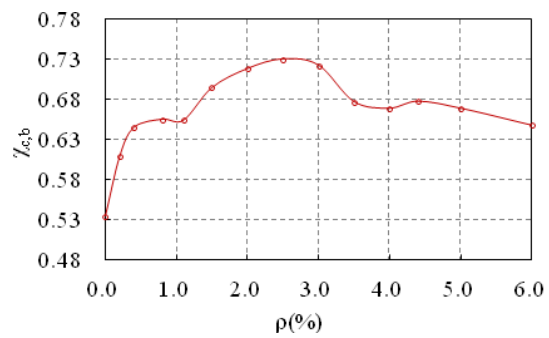


Fig. 12 Bending toughness versus reinforcement ratio

### 3.2.2 Discussions on neutral axis

The results of strain distribution at cross-section when the beams achieved maximum bending strength are plotted in Fig. 13 and the calculated position of neutral axis according to Fig. 13 is listed in Table 2. For the convenience of discussion, the positioning of neutral axis is illustrated in Fig. 14,  $\varphi$  and  $\theta$  is the positioning angle for neutral axis of RCFT and CFT respectively,  $x_o$  and  $x_{oo}$  is the height of neutral axis of RCFT and CFT, respectively.  $x_{oo}$  and  $\varphi$  are all greater than  $x_o$  and  $\theta$  respectively, which means RCFT always has more compressive area than CFT. The increased amount of neutral axis then can be evaluated by

$$\zeta_\varphi = \frac{\varphi}{\theta} \quad \text{or} \quad \zeta_x = \frac{x_o}{x_{oo}} \quad (6)$$

The values of  $\zeta_\varphi$  and  $\zeta_x$  are listed in Table 2 and plotted against  $\rho$  in Fig. 15.  $\zeta_\varphi$  and  $\zeta_x$  is increasing linearly along with the increase of  $\rho$ , which means the compressive area of the beams increase as the amount of axial reinforcements increase.

Based on the regression analysis results of  $\zeta_\varphi$  and  $\zeta_x$ , empirical equations can be proposed as

$$\begin{aligned} \zeta_\varphi &= 0.02\rho + 1.03 \\ \zeta_x &= 0.05\rho + 1.03 \end{aligned} \quad (7)$$

According to discussion results in section 3.2.1,  $\rho$  in Eq. (7) shall be  $1.5\% \leq \rho \leq 3.0\%$ , and correspondingly,  $\zeta_\varphi \leq 1.06$  or  $\zeta_x \leq 1.12$ .

The meaning of Eq. (7) simply is that the total height of compressive area or neutral axis of RCFT increased against CFT by  $\zeta_\varphi$  or  $\zeta_x$  based on the amount of axial reinforcement.

Table 2 Discussions on neutral axis

Labels	$\rho$ (%)	$x_{oo}$ (mm)	$\Phi$ (rad)	$\zeta_\varphi$	$x_o$ (mm)	$\zeta_x$
CFT	0.0	38.22	1.04	1.00	36.78	1.00
PB-R02	0.2	38.08	1.04	1.00	36.92	1.00
PB-R04	0.4	36.80	1.06	1.02	38.20	1.04
PB-R08	0.8	34.99	1.09	1.05	40.01	1.09
PB-R11	1.1	34.57	1.09	1.05	40.43	1.10
PB-R15	1.5	34.53	1.09	1.05	40.47	1.10
PB-R20	2.0	31.86	1.13	1.09	43.14	1.17
PB-R25	2.5	31.47	1.14	1.10	43.53	1.18
PB-R30	3.0	30.20	1.16	1.12	44.80	1.22
PB-R35	3.5	29.78	1.16	1.12	45.22	1.23
PB-R40	4.0	29.13	1.17	1.13	45.87	1.25
PB-R44	4.4	28.20	1.19	1.14	46.80	1.27
PB-R50	5.0	28.00	1.19	1.15	47.00	1.28
PB-R60	6.0	27.15	1.20	1.16	47.85	1.30

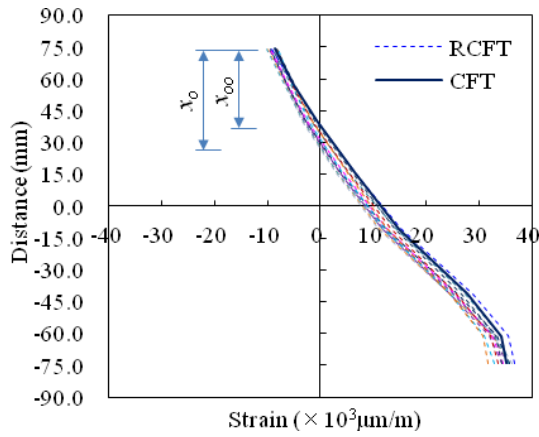


Fig. 13 Strain distribution at maximum bending

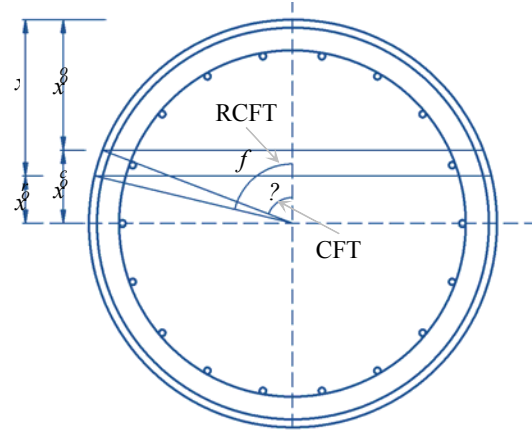
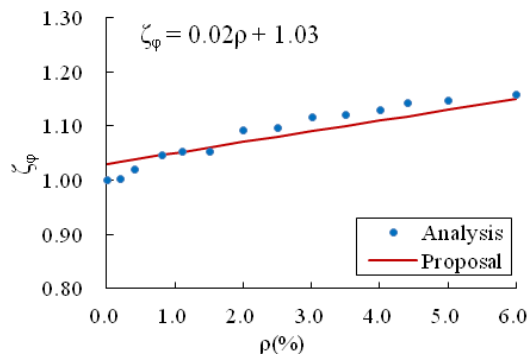
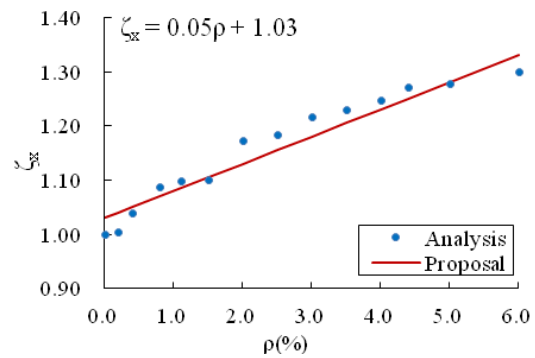


Fig. 14 Illustration of position of neutral axis



(a) Angle of neutral axis



(b) Height of neutral axis

Fig. 15 Effect of axial reinforcement on neutral axis

## 4. Ultimate bending strength of RCFT

### 4.1 Assumptions

Based on the results of experimental studies on CFT and RCFT, following assumptions are supposed:

- (1) Any deformation due to the shear force across the cross-section of the member is not accounted for, namely, the cross-section of CFT and RCFT follows the “plane section assumption”.
- (2) There is no gap between the steel tube and in-filled concrete until the beam reach the maximum bending.
- (3) In-filled concrete stays in a multiaxial stress condition since it is subjected to the confinement pressure imposed by both steel tube and reinforcement, and the compressive strength of in-filled concrete increases compared with its uniaxial stress condition.

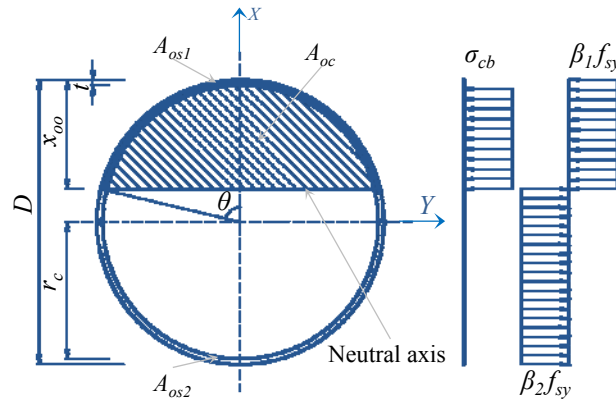


Fig. 16 Stress distribution on cross-section of CFT

- (4) Steel tube stays in a multiaxial elastic-perfectly-plastic stress condition, and the effect of shrinkage and creep of in-filled concrete and local buckling of steel tube can be neglected and follows the von Mises yield condition.
- (5) Tensile strength of in-filled concrete can be ignored.
- (6) The effect of clamping force which is produced by the contact between the steel tube and in-filled concrete on bending strength can be neglected.

#### 4.2 Neutral axis of CFT

When CFT achieves the maximum bending, position of neutral axis and stress distribution on cross-section can be illustrated as Fig. 16.

According to Fig. 16, the equilibrium condition of axial force direction will be

$$\sigma_{cb} \cdot A_{oc} + \beta_1 f_{sy} \cdot A_{os1} = \beta_2 f_{sy} \cdot A_{os2} \quad (8)$$

where  $\sigma_{cb}$  is confined strength of concrete core of CFT, shall be evaluated according to AIJ (2008) as Eq. (9);  $A_{oc} = r_c^2 (\theta - \sin\theta \cos\theta)$  is compression area of concrete core;  $A_{os1} = 2r_c t \theta$  is compression area of steel tube;  $A_{os2} = 2(\pi - \theta)r_c t$  is tension area of steel tube;  $\beta_1$  and  $\beta_2$  is the strength reduction and increase factor for steel tube under compression and tension, respectively, according to AIJ (2008),  $\beta_1 = 0.89$  and  $\beta_2 = 1.08$  for CFT.

$$\sigma_{cb} = \sigma_{co} + 0.78 \cdot \frac{2t}{D - 2t} \cdot f_{sy} \quad (9)$$

Substituting given constants into Eq. (8) leads to

$$\sigma_{cb} r_c^2 (\theta - \sin\theta \cos\theta) + 2r_c t (\beta_1 + \beta_2) f_{sy} \theta = 2\pi r_c t \beta_2 f_{sy} \quad (10)$$

$\theta$  is obtainable from the Eq. (10). Hence, the height or position of neutral axis  $x_{oo}$  of CFT will be

$$x_{oo} = \frac{D}{2} - r_c \cdot \cos \theta \tag{11}$$

### 4.3 Neutral axis of RCFT

#### 4.3.1 Discussions on confinement effect, $\beta_1$ and $\beta_2$

According to former studies (Endo *et al.* 2000, Sato 2008, Tanigaki *et al.* 2002, Suzuki 2008, Wang *et al.* 2002, Wei *et al.* 2005, Xiamuxi and Hasegawa 2011), the mechanical properties of RCFT change significantly compared with CFT, which means the confined strength  $\sigma_c$ ,  $\beta_1$  and  $\beta_2$  should be evaluate differently from CFT.

According to study results of Xiamuxi and Hasegawa (2012), the confine strength  $\sigma_c$  of concrete core of RCFT can be evaluated by

$$\begin{aligned} \sigma_c &= k_c \cdot \sigma_{co} \\ k_c &= 5.71 \cdot \gamma_s^2 - 2.96 \cdot \gamma_s + 1.62 \end{aligned} \tag{12}$$

in which  $\gamma_s$  is the load-sharing ratio of RCFT, considering the effect of axial reinforcement, and can be evaluated by

$$\gamma_s = \frac{N_{so}}{N_{so} + N_{ro} + N_{co}} \tag{13}$$

where  $N_{so} = f_{sy} A_{ss}$  is uniaxial compressive strength of steel tube;  $N_{ro} = f_{sr} A_{sr}$  is uniaxial compressive strength of axial reinforcement;  $N_{co} = \sigma_{co} A_{cc}$  is uniaxial compressive strength of concrete core;  $A_{ss}$ ,  $A_{sr}$  and  $A_{cc}$  are cross-section area of steel tube, axial reinforcement and concrete core, respectively.

According to study results of Xiamuxi and Hasegawa (2012) again, the strength reduction factor  $\beta_1$  for steel tube under compression can be  $\beta_1 = 1.0$  for RCFT. Furthermore, strength increase factor  $\beta_2$  for steel tube under compression can be conservatively set to  $\beta_2 = 1.0$ . Thus, when RCFT achieves the maximum bending, position of neutral axis and stress distribution on cross-section can be illustrated as Fig. 17.

#### 4.3.2 Evaluation of neutral axis of RCFT

According to Fig. 17, the equilibrium condition of axial force direction will be

$$\sigma_c \cdot A_c + f_{sy} \cdot A_{ss1} + f_{sr} \cdot A_{sr1} = f_{sy} \cdot A_{ss2} + f_{sr} \cdot \sum A_{sr2} \tag{14}$$

where  $A_c = r_c^2 (\varphi - \sin \varphi \cos \varphi)$  is compression area of concrete core;  $A_{ss1} = 2r_c t \varphi$  is compression area of steel tube;  $A_{ss2} = 2(\pi - \theta)r_c t$  is tension area of steel tube;  $\sum A_{sr1}$  and  $\sum A_{sr2}$  is the total cross-section area of axial reinforcement in compression and tension, respectively, and  $A_{sr1} = A_{sr2}$  is cross-section area of single reinforcement.

In the Eq. (14), it is difficult to solve exact  $\varphi$  because  $\sum A_{sr1}$  and  $\sum A_{sr2}$  cannot be determined exactly as the position of neutral axis is unknown. Therefore, according discussions in Section 3.2.2, the neutral axial of RCFT can be simplified as

$$\varphi = \zeta_\varphi \cdot \theta = (0.02\rho + 1.03) \cdot \theta \tag{15}$$

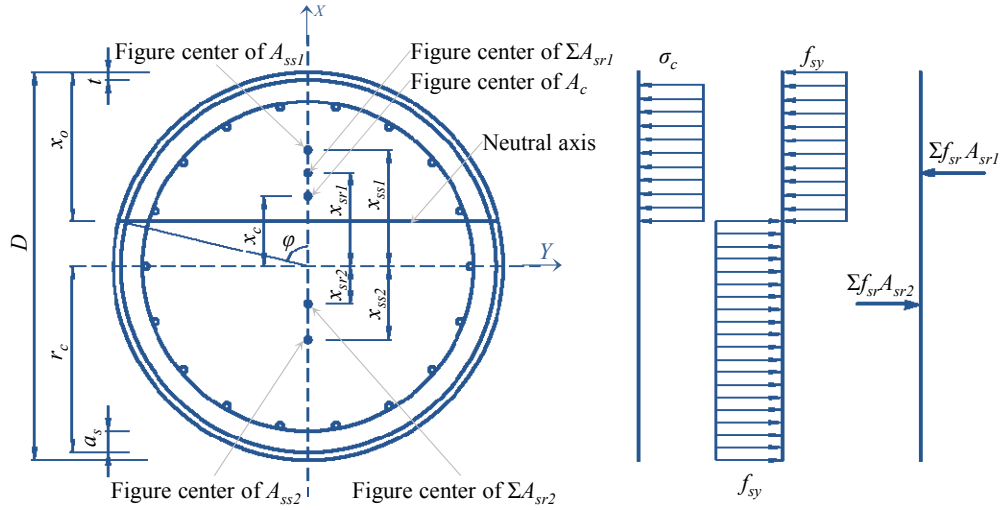


Fig. 17 Stress distribution on cross-section of RCFT

and the height of neutral axis of RCFT will be

$$x_o = \frac{D}{2} - r_c \cdot \cos \varphi \tag{16}$$

#### 4.4 Proposal for bending strength of RCFT

According to Figs. 17 and 18, the distance from the figure center of  $A_c$  to the central axis of cross-section will be

$$x_c = \frac{2r_c^3 \int_{\varphi}^0 \sin \alpha \cos^2 \alpha d\alpha}{A_c} = \frac{2r_c \sin^3 \varphi}{3(\varphi - \sin \varphi \cos \varphi)_c} \tag{17}$$

The distance from the figure center of  $A_{ss1}$  and  $A_{ss2}$  to the central axis of cross-section respectively will be

$$x_{ss1} = \frac{2r_c^2 t \int_0^{\varphi} \cos \alpha d\alpha}{A_{ss1}} = \frac{r_c \sin \varphi}{\varphi} \tag{18}$$

$$x_{ss2} = \frac{2r_c^2 t \int_0^{\pi-\varphi} \cos \alpha d\alpha}{A_{ss2}} = \frac{r_c \sin \varphi}{\pi - \varphi} \tag{19}$$

Furthermore, the distance  $x_{sr1}$  and  $x_{sr2}$  from the figure center of  $\Sigma A_{sr1}$  and  $\Sigma A_{sr2}$  to the central axis of cross-section respectively should be determined according to  $x_o$  (see Eq. (16)) and actual

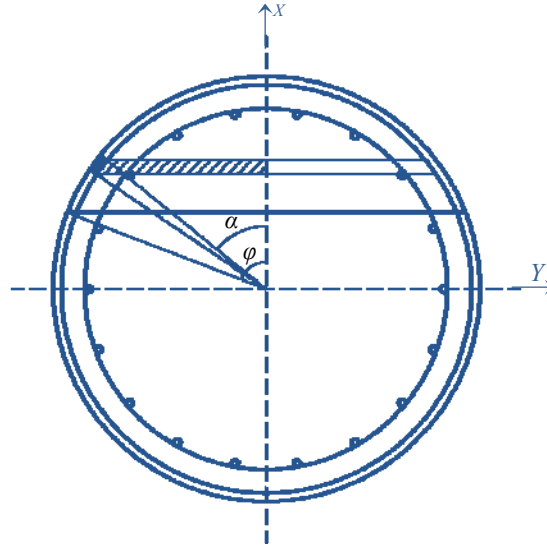


Fig. 18 Determination of figure centers

arrangement of axial reinforcements

According to the equilibrium condition of bending on cross-section in Fig. 17, the ultimate bending strength  $M_u$  of RCFT can be

$$M_u = M_c + M_{ss} + M_{sr} \tag{20}$$

in which  $M_c$  is bending strength of concrete portion

$$M_c = \sigma_c \cdot A_c \cdot x_c = \frac{2}{3} \cdot \sigma_c \cdot r_c^3 \cdot \sin^3 \varphi$$

$M_{ss}$  is bending strength of steel tube portion

$$M_{ss} = f_{sy} \cdot A_{ss1} \cdot x_{ss1} + f_{sy} \cdot A_{ss2} \cdot x_{ss2} = 4 \cdot f_{sy} \cdot r_c^3 \cdot t \cdot \sin \varphi$$

$M_{sr}$  is bending strength of reinforcement portion

$$M_{sr} = f_{sr} \cdot (x_{sr1} \cdot \sum A_{sr1} + x_{sr2} \cdot \sum A_{sr2})$$

## 5. Conclusions

- (1) The ratio of axial reinforcement has the effect on bending performance of RCFT members, and there would be an optimal range for the axial reinforcement ratio of RCFT beams which would help the steel tube and concrete to improve their performance and put RCFT

into better mechanical and economic condition, and this optimal range is proposed as  $1.5\% \leq \rho \leq 3.0\%$ .

- (2) The axial reinforcement has significant effect on the neutral axis of RCFT. RCFT has more compressive area or higher neutral axis than CFT, correspondingly an empirical equation to evaluate the position of neutral axis of RCFT is proposed.
- (3) The effect of axial reinforcement should not be neglected in the evaluation of bending strength of RCFT. Employing the proposed empirical equation for neutral axis of RCFT, an equation in which the effect of axial reinforcement is considered for ultimate bending strength of RCFT is proposed.
- (4) In proposed equation, the bending strength of reinforcement portion needs further studies to simplify the calculation of figure centers of reinforcements, because it may be difficult to determined exact figure centers of reinforcements in case of complicated arrangement of axial reinforcements.

## Acknowledgments

The research described in this paper was financially supported by the Starting-up Research Foundation of Xinjiang University for Doctors.

## References

- ACI Committee 318 (1999), *Building Code Requirements for Structural Concrete and Commentary*, American Concrete Institute, ACI 318-99, Detroit, MI, USA.
- ADINA R&D Inc. (2008), *ADINA Theory and Modeling Guide, Report ARD08-7*, ADINA R&D Inc., Watertown, New York, NY, USA.
- AIJ (2008), *Recommendations for Design and Construction of Concrete Filled Steel Tubular Structures*, Architectural Institute of Japan, Tokyo, Japan.
- ASCE (1982), *ASCE Task Committee on Concrete and Masonry Structure, State of the Art Report on Finite Element Analysis of Reinforced Concrete*, ASCE, New York, NY, USA.
- Chen, S.C., Ren, A.Z., Wang, J.F. and Lu, X.Z. (2008), "Numerical modeling of reinforced concrete slabs subjected to fire", *Eng. Mech.*, **25**(3), 107-112.
- Choi, K.K. and Yan, X. (2010), "Analytical model of circular CFRP confined concrete-filled steel tubular columns under axial compression", *J. Compos. Construct., ASCE*, **14**(1), 125-128.
- Endo, T., Shioi, Y., Hasegawa, A. and Wang, H.J. (2000), "Experimental study on reinforced concrete filled steel tubular structure", *Proceedings of the 7th International Conference on Steel Structures*, Singapore, July.
- Han, L.H., Yao, G.H. and Tao, Z. (2007), "Performance of concrete-filled thin-walled steel tubes under pure torsion", *Thin-Wall. Struct.*, **45**(1), 24-36.
- Hou, C.C., Han, L.H. and Tao, Z. (2011), "Simulation on concrete-filled steel tubular members under transverse impact", *The 2011 World Congress on Advances in Structural Engineering and Mechanics (ASEM11<sup>+</sup>)*, Seoul, Korea, September.
- Hu, H.T., Huang, C.S. and Wu, M.H. (2003), "Nonlinear analysis of axially loaded concrete-filled tube columns with confinement effect", *J. Struct. Eng., ASCE*, **129**(10), 1322-1329.
- JSCE (2007), *Standard Specifications for Concrete Structures-2007, Design*, Japan Society of Civil Engineers, Tokyo, Japan.
- JSCE 9-A (1999), *Theory and Design of Steel-concrete Hybrid Structures*, Japan Society of Civil Engineers, Tokyo, Japan.

- Kupfer, H., Hilsdorf, H.K. and Rush, H. (1969), "Behavior of concrete under biaxial stresses", *ACI J.*, **66**(8), 656-666.
- Kwak, H.G., Kwak, J.H. and Gang, H.G. (2011), "Cyclic behavior of circular concrete filled steel tubular column", *The 2011 World Congress on Advances in Structural Engineering and Mechanics (ASEM 11<sup>+</sup>)*, Seoul, Korea, September.
- Mao, P.F. and Wang, D.L. (2011), "Nonlinear finite element modeling of the interior steel-concrete composite beam joints", *Int. J. Nonlinear Sci.*, **11**(2), 173-179.
- Patel, V.I., Liang, Q.Q. and Hadi, M.N.S. (2012), "Inelastic stability analysis of high strength rectangular concrete-filled steel tubular slender beam-columns", *Interact. Multiscale Mech., Int. J.*, **5**(2), 91-104.
- Sato, M. (2008), "Study on structural characteristics of RCFT and the application to practical structures", M.S. Dissertation, Hachinohe Institute of Technology, Hachinohe, Japan.
- Soranakom, C. and Mobasher, B. (2007), "Flexural modeling of strain softening and strain hardening fiber reinforced concrete", *RILEM Proceedings, Pro. 53, S.A.R.L.*, Cachan, France, July.
- Suzuki, T. (2008), "Study on new bridges that adopt hybrid structure", Ph.D. Dissertation, Hachinohe Institute of Technology, Hachinohe, Japan.
- Tanigaki, K., Kanai, T. and Komuro, T. (2002), "Construction of high-rise building using reinforced concrete columns formed in steel tube (RCFT) structural system", *AIJ J. Tech. Des.*, **16**, 23-26.
- Wang, H.J., Ishibashi, H., Wei, H. and Hasegawa, A. (2002), "Experimental study on twin-column RCFT pier", *The Second International Conference on Advances in Structural Engineering and Mechanics (ASEM 02)*, Seoul, Korea, September.
- Wei, H., Wang, H.J., Hasegawa, A. and Shioi, Y. (2005), "Study on strength of reinforced concrete filled circular steel tubular columns", *Struct. Eng. Mech., Int. J.*, **19**(6), 653-677.
- Xiamuxi, A. and Hasegawa, A. (2011), "Experimental study on reinforcement ratio of RCFT columns under axial compression", *Adv. Mater. Res.*, **250-253**, 3790-3797.
- Xiamuxi, A. and Hasegawa, A. (2012), "A study on axial compressive behaviors of reinforced concrete filled tubular steel columns", *J. Construct. Steel Res.*, **76**, 144-154.
- Zeng, Y., Leung, C.C.Y. and Au, F.T.K. (2011), "Finite element analysis of in-situ stitches in precast concrete segmental bridges", *The 2011 World Congress on Advances in Structural Engineering and Mechanics (ASEM 11<sup>+</sup>)*, Seoul, Korea, September.